Bayesian parameter estimation and model comparison for $^{14}\mathrm{C}(n,\gamma)^{15}\mathrm{C}$

Timothy Lund[1,*] and Gautam Rupak[2,†]

[1] *Houghton College, Houghton, NY 14744, USA*

[2] *Department of Physics & Astronomy and HPC[2] Center for Computational Sciences, Mississippi State University, Mississippi State, MS 39762, USA*

(Dated: February 10, 2023)

Bayesian method is used to study the low energy reaction $^{14}\mathrm{C}(\mathrm{n},\gamma)^{15}\mathrm{C}$.

I. INTRODUCTION

Nuclear reactions fuels the stars and determine stellar evolution. *p*-*p* fusion and catalytic Carbon-Nitrogen-Oxygen (CNO) cycle are the two prominent sources of energy generation in the stars. Stellar models depend on low energy nuclear cross section inputs. Cross section measurements, especially involving charged nuclei, at astrophysical energies are difficult and often unavailable. For radiative capture reactions $a(b,\gamma)c$ where a, b, c are light nuclei, the inverse process $c(\gamma^*,b)a$ can be measured through Coulomb dissociation (CD) by a virtual photon γ^* of the strong electromagnetic field generated by another heavy source nuclei with a large charge. However, the kinematics accessible in CD might not always overlap with the region of interest, and possibly probe nuclear channels that are different than the direct capture (DC) process one is interested in. Thus theoretical input is often needed to interpret CD data. Theory is also needed to extrapolate DC data from the measured energies to the low energy of astrophysical interest.

Astrophysics interest in $^{14}\mathrm{C}(\mathrm{n},\gamma)^{15}\mathrm{C}$ includes its role as the slowest reaction in the neutron induced CNO cycle in helium-burning layers of asymptotic giant branch stars. This slow reactions is a bottle neck in the production of nuclei with mass number $A \geq 14$ in Big Bang Nucleosynthesis. Experimental interest in this reaction stems from the fact that both DC and CD measurements probe overlapping kinematical regions that can be a useful tool to compare, improve and validate the two alternate methods of measurements. [Fill in some history of experiments]

Stellar models require accurate nuclear cross section inputs. This necessitates theory extrapolations with reliable error estimates. Effective field theory (EFT) provides a framework that is model-independent with quantifiable error estimates well suited for low energy reaction calculations.

Halo EFT as the name suggests is used to describe structure and reactions involving halo nuclei that are described as a shallow bound system of a single or more valance nucleons and a tightly bound core. The small valance nucleon separation energy compared to the typical binding or excitation energy of the core is used to define a small ratio for the perturbative halo EFT calculation.

The $^{15}\mathrm{C}$ nuclei with a neutron separation energy $B = 1.218\,\mathrm{MeV}$ is described as a single neutron halo with a tightly bound $^{14}\mathrm{C}$ core with excitation energy $E_\star \approx 6\,\mathrm{MeV} \gg B$. At the low energies relevant for the CNO cycle, the cross section is not expected to be sensitive to the structure of the core, and a two-cluster $n+^{14}\mathrm{C}$ description is expected to be sufficient. This system is ideal to test out not only different experimental methods but also the halo EFT formalism which benefits from the separation in scales between the small binding energy B, low scattering energy and the high excitation and breakup energy of the tight $^{14}\mathrm{C}$ core.

The calculation of the $^{14}\mathrm{C}(\mathrm{n},\gamma)^{15}\mathrm{C}$ reaction requires accurate description of the incoming $n+^{14}\mathrm{C}$ state, the final $^{15}\mathrm{C}$ bound state, and the electromagnetic (EM) transition operator. The EM operators at the lowest order of perturbation in EFT are given by one-body currents that are well constrained by gauge symmetry. The final bound state and incoming scattering state can both be described model-independently in terms of a few scattering parameters at low energy that appear in the effective range expansion (ERE). In this work we revisit the radiative capture $^{14}\mathrm{C}(\mathrm{n},\gamma)^{15}\mathrm{C}$ capture calculation in halo EFT. The scattering parameters in the initial and final states are not well known. This leads to ambiguity in the construction of the low energy theory. Both the DC and CD data requires enhancement of some operators in the initial state and/or final state interaction. Ref. [1] considered a particular enhancement of initial state *p*-wave interactions and Ref. [2] considered another enhancement of *s*-wave final state interactions both of which gave compatible accurate description of data. A quantitative comparison of the two EFT formulations [1, 2] is provided here using Bayesian model comparison [3]. [Write something about the need to do this kind of theory comparisons]

We start with some basic definitions from Bayesian statistics relevant for theory comparisons in section II. We discuss the calculation of evidence for a theory from the available data, and how it is used to calculate the posterior odds in favor or against a theory in comparison to another. In section III, we present the EFT expressions for the $^{14}\mathrm{C}(\mathrm{n},\gamma)^{15}\mathrm{C}$ cross section derived earlier in Refs. [1, 2]. We further develop the power counting for the two EFT formulations to compare them up to next-to-leading order (NLO) in the perturbative expansion.

* timothy.lund23@houghton.edu

† grupak@ccs.msstate.edu

II. BAYESIAN METHOD

The cross section contains a number of parameters that cannot be determined theoretically. Previous parameter estimations in [1] utilized χ^2 minimization, which maximizes the likelihood function $P(D|\theta, H)$ by the relation $\chi^2 \propto -\ln P(D|\theta, H)$. The likelihood is given by

$$P(D|\theta, H) = \prod_{i=1}^{N} \frac{1}{\sigma_i\sqrt{2\pi}} \exp\left\{-\frac{(y_i - \mu_i(\theta))^2}{2\sigma_i^2}\right\}, \quad (1)$$

where data set D consists of N measurements y_i with corresponding errors σ_i. Theory predictions $\mu_i(\theta)$ are determined by model parameters θ.

We consider Bayesian methods as as an alternative to χ^2 because they allow us to naturally incorporate prior assumptions about the parameter ranges into model fitting. Additionally, Bayesian methods allow us to compare different models by calculating the evidence from the data in favor of each one.

Bayes' theorem is given by

$$P(\theta|D, H) = \frac{P(D|\theta, H)P(\theta|H)}{P(D|H)}, \quad (2)$$

where the posterior $P(\theta|D, H)$ is the probability of parameters θ defining the distribution of D. Parameter constraints are incorporated using the prior distribution $P(\theta|H)$; we take this to be a uniform distribution over the theoretical parameter ranges.

The evidence $P(D|H)$ is given by

$$P(D|H) = \int P(D|\theta, H)P(\theta|H)d\theta. \quad (3)$$

As such, it is also often referred to as the marginal likelihood. In the context of Bayes' theorem, the evidence is the normalization constant that sets the area under $P(\theta|D, H)$ to unity.

Bayesian evidence calculation allows us to compare models with different parameter spaces. Suppose we have models A and B, denoted M_A and M_B; we can compare the two using the posterior odds ratio

$$\frac{P(M_A|D, H)}{P(M_B|D, H)} = \frac{P(D|M_A, H)}{P(D|M_B, H)} \cdot \frac{P(M_A|H)}{P(M_B|H)}, \quad (4)$$

where first term on the right-hand side is the ratio of evidences. The second term on the right is known as the prior odds ratio, which reflects prior assumptions about which model is more likely to express the distribution of the data. For our purposes, we consider the prior odds ratio to be unity.

With a χ^2 minimization, increasing the number of model parameters may yield a better fit. However, Bayesian evidence balances a model's wellness-of-fit with its simplicity, using a natural implementation of Occam's razor [4]. Adding more parameters introduces more priors over which to marginalize, thus penalizing needless complexity.

For models with multiple parameters, calculating Bayesian evidence becomes a multi-dimensional integration problem that can be difficult to solve. Thus, we utilize a Markov-Chain Monte Carlo method known as Nested Sampling to estimate the evidence.

Nested sampling maps the likelihood function in multidimensional parameter space onto a number line between 0 and 1. The lowest likelihood is mapped to 1 and the highest is mapped to 0. n "live" points are drawn from parameter space, and the likelihood for each is calculated. The "worst" point (the one with the lowest likelihood value) is mapped onto the number line. It is then replaced by sampling another point with a greater likelihood. The number line is iteratively populated with the worst likelihood values in this way, ultimately allowing us to calculate evidence using a simple integration in one dimension.

Sampling to replace the worst point may be done using various methods, including the Metropolis-Hastings algorithm. We implement Nested Sampling using the Nestle library in Python, which samples using multiple ellipsoids in parameter space that bound the live points [5].

III. EFFECTIVE FIELD THEORY

The spin-parity J^π assignments of the incoming neutron n and ^{14}C nuclei are $\frac{1}{2}^+$ and 0^+, respectively. The ground state of ^{15}C is a $\frac{1}{2}^+$ which is described as a s-wave bound state of n and ^{14}C in halo EFT. We consider E1 capture from initial p-wave states that can be in the $^2P_{1/2}$ and $^2P_{3/2}$ states using the spectroscopic notation $^{2S+1}L_J$ for total channel spin S, orbital momentum L and angular momentum J. The various expressions in this section are taken from Ref. [1] where the reader can find more details about the calculation.

The relevant interaction for the capture reaction ^{14}C(n, γ)^{15}C is given by

$$\mathcal{L} = n_\alpha^\dagger \left[i\partial_0 + \frac{\nabla^2}{2m_n}\right] n_\alpha + C^\dagger \left[i\partial_0 + \frac{\nabla^2}{2m_c}\right] C + \mathcal{L}_s + \mathcal{L}_p\,, \quad (5)$$

where n is the nucleon field with spin label α and mass $m_n = 939.6$ MeV. Sum over repeated indices implied unless stated otherwise. C is the spinless field representing the ^{14}C core with mass $m_c = 13044$ MeV. We use natural units where $\hbar = 1 = c$. The interaction in the $^2S_{1/2}$ ground state channel is given by

$$\mathcal{L}_s = \phi_\alpha^\dagger \left[\Delta^{(0)} + i\partial_0 + \frac{\nabla^2}{2M}\right] \phi_\alpha + h^{(0)} \left[\phi_\alpha^\dagger (n_\alpha C) + \text{h.c.}\right]. \quad (6)$$

An auxiliary field of total mass $M = m_n + m_c$ with the quantum numbers of the ground state ^{15}C is usually introduced for convenience. The p-wave interactions are given by

$$\mathcal{L}_p = \sum_{\eta=1}^{2} \chi_i^{\alpha,\eta\dagger}\left[\Delta^{(\eta)} + i\partial_0 + \frac{\nabla^2}{2M}\right]\chi_i^{\alpha,\eta} + \sum_{\eta=1}^{2} h^{(\eta)}[\chi_i^{\alpha,\eta\dagger} P_{ik}^{\alpha\gamma,\eta} N_\gamma \left(\frac{\overrightarrow{\nabla}}{m_c} - \frac{\overleftarrow{\nabla}}{m_n}\right)_k C + \mathrm{h.c}] \,, \quad (7)$$

where $\eta = 1, 2$ correspond to the ${}^2P_{1/2}$ and ${}^2P_{3/2}$ channels, respectively. The p-wave projectors for the $J = 1/2$ and $J = 3/2$ channels are defined as

$$\begin{aligned} P_{ij}^{\alpha\beta,1} &= \frac{1}{\sqrt{3}}(\sigma_i\sigma_j)^{\alpha\beta} \,, \\ P_{ij}^{\alpha\beta,2} &= \sqrt{3}\delta_{ij}\delta^{\alpha\beta} - \frac{1}{\sqrt{3}}(\sigma_i\sigma_j)^{\alpha\beta} \,. \end{aligned} \quad (8)$$

The auxiliary fields ϕ, and χ can be integrated out of the theory using the equation of motion, leaving only four-particle interactions between the neutron and ^{14}C core.

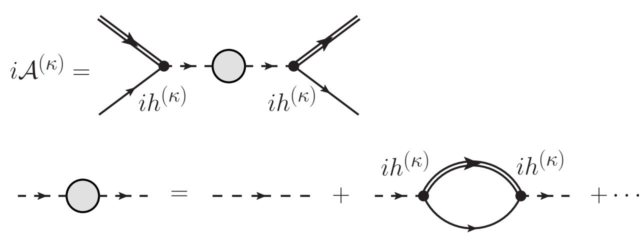

FIG. 1. [Change wording a little] Elastic scattering amplitudes $\mathcal{A}^{(\kappa)}$ in s- and p-waves. Double line is the ^{14}C propagator, single line the neutron propagator, dashed line the bare dimer propagator. $\kappa = 0, 1, 2$ corresponds to ${}^2S_{1/2}$, ${}^2P_{1/2}$ and ${}^2P_{3/2}$ channels, respectively.

The elastic-scattering amplitude in halo EFT in the s and p waves can be calculated from the diagrams in Fig. 1 using the interactions in Eqs. (6), (7). The scattering amplitudes describes both the incoming and the final bound states. At low energies, the scattering amplitude can be expressed model-independently in terms of a few scattering parameters using the effective range expansion (ERE) as

$$\begin{aligned} i\mathcal{A}_l(p) &= \frac{2\pi}{\mu}\frac{i}{p\cot\delta_l - ip} \,, \\ p^{2l+1}\cot\delta_l &\approx -1/a_l + \frac{1}{2}r_l p^2 + \dots \,, \end{aligned} \quad (9)$$

for the l-th partial wave. The dimensionful scattering parameters a_l, r_l determined by the short-ranged nuclear interaction with a range set by the inverse of the physical cutoff Λ. Accordingly, the natural expectation is that a_l, r_l are given by some powers of Λ up to numerical factors of order 1. However, we will consider a couple of situations where some of the scattering parameters are fine-tuned and enhanced by factors of Q instead of Λ. The ERE parameters are used to determine the EFT couplings, and accordingly we consider different power-counting based on the sizes of the ERE parameters.

A straightforward calculation in s wave gives the EFT amplitude

$$i\mathcal{A}_0(p) = \frac{-i[h^{(0)}]^2}{\Delta^{(0)} + \frac{p^2}{2\mu} + \frac{\mu}{2\pi}[h^{(0)}]^2(\lambda + ip)} \,, \quad (10)$$

where λ is a renormalization scale introduced to regulate divergences in the EFT calculation. Physical observables are independent of λ. In the s-wave, we rearrange the ERE to make the pole in the scattering amplitude explicit at $p = i\gamma$ where γ is the binding momentum by writing

$$p\cot\delta_0 \approx -\gamma + \frac{1}{2}\rho(p^2 + \gamma^2) + \dots \,. \quad (11)$$

From Eqs. (9), (10) and (11), we fix the ERE couplings $\Delta^{(0)}$, $h^{(0)}$ as

$$\begin{aligned} \frac{2\pi\Delta^{(0)}}{\mu[h^{(0)}]^2} + \lambda &= \gamma - \frac{1}{2}\rho\gamma^2 \,, \\ -\frac{2\pi}{[h^{(0)}]^2\mu^2} &= \rho \,. \end{aligned} \quad (12)$$

At low energy the contribution of the ^{15}C bound state wave function is contained in two parameters: the binding momentum γ which appears as a pole in the amplitude $\mathcal{A}_0$ at energy $E = -B$ (or momentum $p = i\gamma$) and the residue at this pole. In writing the ERE around the pole $p = i\gamma$ in Eq. (11), the reside is determined once the effective range ρ is known. Typically one calculates the wave function renormalization constant $\mathcal{Z}$ from the residue at the pole as

$$[h^{(0)}]^{-2}\mathcal{Z}^{-1} = -\frac{\partial}{\partial E}\frac{1}{\mathcal{A}_0(p)}\Big|_{E=-B} = \frac{\mu^2}{2\pi}\frac{1-\rho\gamma}{\gamma} \,. \quad (13)$$

The capture cross section depends on the combination $[h^{(0)}]^2\mathcal{Z}$ which can also be related to the Asymptotic Normalization Constant (ANC) of the s-wave bound state wave function as

$$C_{1,s}^2 = \frac{\mu^2}{\pi}[h^{(0)}]^2\mathcal{Z} = \frac{2\gamma}{1-\rho\gamma} \,. \quad (14)$$

The bound state can be model-independently specified at low energy in terms of the two scattering parameters γ and ρ.

The p-wave amplitude is calculated in EFT as

$$i\mathcal{A}_1^{(\eta)}(p) = \frac{i2\pi p^2/\mu}{-\frac{2\pi\mu\Delta^{(\eta)}}{[h^{(\eta)}]^2} - \frac{\pi\lambda^3}{2} - \left(\frac{3\lambda}{2} + \frac{\pi}{[h^{(\eta)}]^2}\right)p^2 - ip^3} \,. \quad (15)$$

Matching Eqs. (15) and (9), we get for p waves

$$\begin{aligned} -\frac{2\pi\mu\Delta^{(\eta)}}{[h^{(\eta)}]^2} - \frac{\pi}{2}\lambda^3 &= -1/a_1^{(\eta)} \,, \\ -\frac{3}{2}\lambda - \frac{\pi}{[h^{(\eta)}]^2} &= \frac{1}{2}r_1^{(\eta)} \,, \end{aligned} \quad (16)$$

that determines the p-wave EFT couplings $\Delta^{(\eta)}$, $h^{(\eta)}$ from the scattering parameters $a_1^{(\eta)}$, $r_1^{(\eta)}$. In the ${}^2P_{1/2}$ there is a resonance at $E_r \approx 1.885$ MeV with width $\Gamma_r \approx 40$ keV in the cm frame. As one approaches the resonance from $E < E_r$, the phase shift $\delta_1^{(1)}$ passes through $\pi/2$ from below i.e. $\cot\delta_1^{(1)}(E_r) = 0$ and $\cot'\delta_1^{(1)}(E_r) < 0$. Defining $\cot'\delta_1^{(1)}(E_r) \equiv -2/\Gamma_r$ we calculate [6] the scattering parameters in this channel as

$$a_1^{(1)} = -\frac{\mu\Gamma_r}{p_r^5}, \quad \text{and} \quad r_1^{(1)} = -\frac{2p_r^3}{\mu\Gamma_r}, \tag{17}$$

that gives a results in a Breit-Wigner form with a width Γ_r for the amplitude $\mathcal{A}_1^{(1)}$ near the resonance energy E_r. p-wave resonance in n-α scattering was considered in Refs. [7, 8] using halo EFT. It was shown that non-perturbative treatment of the scattering volume a_1 and effective momentum r_1 in a p-wave channel is necessary to describe a resonance.

The scattering parameters $a_1^{(2)}$, $r_1^{(2)}$ in the ${}^2P_{3/2}$ are not known which becomes an unknown source of uncertainty in the calculation, along with the ${}^2S_{1/2}$ effective range ρ. The one-body current for E1 capture are obtained by gauging the ^{14}C core derivatives/momentum with minimal substitution $\boldsymbol{q} \to \boldsymbol{q} + eZ_c\boldsymbol{A}$ where $\boldsymbol{A}$ is the vector potential, $Z_c = 6$ and e the proton charge. The total capture cross section is then calculated as [6]

$$\begin{aligned}
\sigma(p) &= \frac{1}{2}\frac{64\pi\alpha}{M_c^2\mu^2}\frac{p\gamma(p^2+\gamma^2)}{1-\rho\gamma}\sum_{\eta=1}^{2}(2J^{(\eta)}+1)|g^{(\eta)}(p)|^2\,,\\
g^{(\eta)}(p) &= \frac{\mu}{p^2+\gamma^2} + \frac{6\pi\mu}{-1/a_1^{(\eta)} + r_1^{(\eta)}p^2/2 - ip^3}\\
&\qquad\times\left[\frac{\gamma}{4\pi} + \frac{ip^3-\gamma^3}{6\pi(p^2+\gamma^2)}\right].
\end{aligned}\tag{18}$$

The angular momentum $J^{(1)} = 1/2$ and $J^{(2)} = 3/2$ in the ${}^2P_{1/2}$ and ${}^2P_{3/2}$ channels respectively.

[Discuss the two power countings next.]

IV. ANALYSIS

We fit data in Region I ($E_{\rm cm} \lesssim 1\,$MeV) that involves 10 Nakamura data points, and in Region II ($E_{\rm cm} \lesssim 2.0\,$MeV) that involves 18 Nakamura data points [9]. The 4 data points from Reifarth et al. are below $E_{\rm cm} \lesssim 1\,$MeV [10]. We perform fits both with and without the lowest energy Reifarth data point, thus giving us a total of 4 different kinds of fits. The fits that include the lowest Reifarth data are indicated with a $\star$.

The χ^2 fit in Ref. [1] corresponds to a LO calculation in EFT A power counting that found $a_1^{(2)} \sim -1.3\times10^{-5}\,\text{MeV}^{-3} \sim Q^{-3}$, $r_1^{(2)}/2 \sim 45\,\text{MeV} \sim Q$. This power counting assumes natural-sized $\rho \sim 1/\Lambda$, $s_1^{(2)} \sim 1/\Lambda$ at NLO. Accordingly, we choose the priors

$$\begin{aligned}
\rho &\sim U(-2\,\text{fm}, 2\,\text{fm})\,,\\
a_1^{(2)} &\sim U(-5Q^{-3}, 5Q^{-3})\,,\\
r_1^{(2)} &\sim U(0, 5Q)\,,\\
s_1^{(2)} &\sim U(-2/\Lambda, 2/\Lambda)\,,
\end{aligned}\tag{19}$$

where we use $Q = 40\,$MeV, $\Lambda = 200\,$MeV in the fits. A wider prior range including possible negative $r_1^{(2)} < 0$ values does not impact the quality of those fits that seem to suggest that $r_1^{(2)} > 0$. Further, restricting the fits to negative $a_1^{(2)} < 0$ values, based on previous information from the χ^2 fit, is possible even though we use a wider prior range. The subsequent work in Ref. [2] considered the alternate power counting with a larger s-wave effective range $\rho \sim 1/Q$ that contributes at LO. The initial state p-wave interaction in the $2P_{3/2}$ channel was relegated to higher order. A χ^2 fit gave $\rho \sim 2.76\,$fm. As discussed earlier, natural sized p-wave scattering parameters $a_1^{(2)} \sim \Lambda^{-3}$, $r_1^{(2)} \sim \Lambda$ would push the initial state interaction to N^{3}LO. We consider the possible single p-wave fine tuning suggested in Ref. [8] where $a_1^{(2)} \sim Q^{-2}\Lambda^{-1}$. This makes initial state contribution NLO. We use the prior

$$\begin{aligned}
\rho &\sim U(0, 4.2\,\text{fm})\,,\\
a_1^{(2)} &\sim U(-2Q^{-2}\Lambda^{-1}, 2Q^{-2}\Lambda^{-1})\,,\\
r_1^{(2)} &\sim U(\Lambda/2, 2.5\Lambda)\,.
\end{aligned}\tag{20}$$

Physics demands that the wave function renormalization $\mathcal{Z}$ (or the ANC) be positive, and accordingly $\rho < 1/\gamma \sim 4.3\,$fm. Moreover, in the EFT B, we expect a larger ANC which requires $\rho > 0$. Note that the choice of prior in EFT B allows the possibility of natural sized $a_1^{(2)} \sim Q^{-3}$.

As reference, we also fit the EFT expressions without any power counting expansion (without the shape parameter terms) in the 4 previously-mentioned fits over a wider prior range:

$$\begin{aligned}
\rho &\sim U(-5\,\text{fm}, 4.2\,\text{fm})\,,\\
a_1^{(2)} &\sim U(-10Q^{-3}, 10Q^{-3})\,,\\
r_1^{(2)} &\sim U(0, 2.5\Lambda)\,.
\end{aligned}\tag{21}$$

These fits are called EFT$_{\text{all}}$. We do not include the shape parameter $s_1^{(2)}$ in these fit that do not follow any specific power counting. From the NLO EFT A fits III, we find that $s_1^{(2)}$ is poorly constrained by the available data and it is consistent with being zero.

I observed the following:

1. Usually, LO EFT B gives the strongest evidence but overall EFT B is better than EFT A.

2. When the errors in the parameters are skewed it is usually due to a bi-modal distribution such as for ρ at NLO B.

3. Larger ρ is associated with smaller $|a_1^{(2)}|$, and smaller ρ with larger $|a_1^{(2)}|$, indicative of the two alternate but similar χ^2 fits.

4. $a_1^{(2)}$ is more sensitive to the momentum dependence of data whereas ρ only effects the overall normalization.

5. Keeping the lowest Reifarth data in EFT B NLO fits bring the bi-model nature into focus though overall the NLO fit has large uncertainties in the parameters. Without the lowest point, ρ has a large distribution covering the bi-modal region of the previous fit.

6. All the fitted parameters are consistent with their respective power counting estimates, though some with large uncertainty.

7. EFT B describes data better. If we want to constrain theory better at NLO, we need better low-energy data.

V. CONCLUSIONS

[1] G. Rupak, L. Fernando, and A. Vaghani, Phys. Rev. C **86**, 044608 (2012), arXiv:1204.4408 [nucl-th].

[2] L. Fernando, A. Vaghani, and G. Rupak, (2015), arXiv:1511.04054 [nucl-th].

[3] P. Premarathna and G. Rupak, Eur. Phys. J. A **56**, 166 (2020), arXiv:1906.04143 [nucl-th].

[4] D. S. Sivia and J. Skilling, *Data Analysis - A Bayesian Tutorial*, 2nd ed., Oxford Science Publications (Oxford University Press, 2006) p. 81.

[5] F. Feroz, M. P. Hobson, and M. Bridges, Monthly Notices of the Royal Astronomical Society **398**, 1601–1614 (2009).

[6] L. Fernando, R. Higa, and G. Rupak, Eur. Phys. J. A **48**, 24 (2012), arXiv:1109.1876 [nucl-th].

[7] C. A. Bertulani, H. W. Hammer, and U. Van Kolck, Nucl. Phys. A **712**, 37 (2002), arXiv:nucl-th/0205063.

[8] P. F. Bedaque, H. W. Hammer, and U. van Kolck, Phys. Lett. B **569**, 159 (2003), arXiv:nucl-th/0304007.

[9] T. Nakamura *et al.*, Phys. Rev. C **79**, 035805 (2009).

[10] R. Reifarth *et al.*, Phys. Rev. C **77**, 015804 (2008), arXiv:0910.0106 [astro-ph.IM].

TABLE I. Fitted parameters using the prior set 1. Seed=1234

Theory	ρ (fm)	$a_1^{(2)}$ (MeV^{-3})	$r_1^{(2)}$ (MeV)	$s_1^{(2)}$ (MeV^{-1})	s_1	s_2
$\mathrm{EFT}^{\star}_{\mathrm{all}}$ I	$1.63^{+0.27}_{-0.45}$	$-1.26\times10^{-5}{}^{+2.78\times10^{-6}}_{-3.20\times10^{-6}}$	384^{+79}_{-120}	—	$1.05^{+0.05}_{-0.05}$	$0.9^{+0.04}_{-0.04}$
$\mathrm{EFT}^{\star}_{\mathrm{A}}$ LO I	—	$-2.12\times10^{-5}{}^{+1.70\times10^{-6}}_{-1.93\times10^{-6}}$	156^{+19}_{-18}	—	$1.03^{+0.04}_{-0.04}$	$0.89^{+0.04}_{-0.04}$
$\mathrm{EFT}^{\star}_{\mathrm{A}}$ NLO I	$0.6^{+0.45}_{-0.48}$	$-1.84\times10^{-5}{}^{+2.63\times10^{-6}}_{-3.02\times10^{-6}}$	178^{+15}_{-24}	$-1.15\times10^{-3}{}^{+7.10\times10^{-3}}_{-5.77\times10^{-3}}$	$1.06^{+0.04}_{-0.04}$	$0.89^{+0.04}_{-0.04}$
$\mathrm{EFT}^{\star}_{\mathrm{B}}$ LO I	$2.79^{+0.06}_{-0.07}$	—	—	—	$1.08^{+0.05}_{-0.05}$	$0.87^{+0.04}_{-0.04}$
$\mathrm{EFT}^{\star}_{\mathrm{B}}$ NLO I	$2.73^{+0.14}_{-0.49}$	$-2.30\times10^{-7}{}^{+5.90\times10^{-7}}_{-5.11\times10^{-6}}$	363^{+101}_{-170}	—	$1.08^{+0.04}_{-0.04}$	$0.87^{+0.03}_{-0.03}$
$\mathrm{EFT}_{\mathrm{all}}$ I	$1.64^{+0.39}_{-0.69}$	$-9.60\times10^{-6}{}^{+3.91\times10^{-6}}_{-4.69\times10^{-6}}$	311^{+131}_{-123}	—	$1.04^{+0.05}_{-0.05}$	$0.91^{+0.04}_{-0.04}$
$\mathrm{EFT}_{\mathrm{A}}$ LO I	—	$-1.72\times10^{-5}{}^{+2.23\times10^{-6}}_{-2.38\times10^{-6}}$	128^{+21}_{-21}	—	$1.03^{+0.05}_{-0.05}$	$0.9^{+0.04}_{-0.04}$
$\mathrm{EFT}_{\mathrm{A}}$ NLO I	$0.89^{+0.65}_{-0.78}$	$-1.36\times10^{-5}{}^{+3.09\times10^{-6}}_{-3.86\times10^{-6}}$	162^{+25}_{-38}	$-8.86\times10^{-4}{}^{+6.47\times10^{-3}}_{-6.23\times10^{-3}}$	$1.04^{+0.05}_{-0.05}$	$0.91^{+0.04}_{-0.04}$
$\mathrm{EFT}_{\mathrm{B}}$ LO I	$2.74^{+0.07}_{-0.08}$	—	—	—	$1.05^{+0.05}_{-0.05}$	$0.91^{+0.04}_{-0.04}$
$\mathrm{EFT}_{\mathrm{B}}$ NLO I	$2.31^{+0.32}_{-0.24}$	$-2.90\times10^{-6}{}^{+2.41\times10^{-6}}_{-2.27\times10^{-6}}$	337^{+105}_{-133}	—	$1.05^{+0.05}_{-0.05}$	$0.91^{+0.04}_{-0.04}$
$\mathrm{EFT}^{\star}_{\mathrm{all}}$ II	$1.73^{+0.23}_{-0.3}$	$-1.05\times10^{-5}{}^{+2.39\times10^{-6}}_{-2.76\times10^{-6}}$	399^{+70}_{-101}	—	$1.03^{+0.05}_{-0.05}$	$0.89^{+0.04}_{-0.04}$
$\mathrm{EFT}^{\star}_{\mathrm{A}}$ LO II	—	$-1.90\times10^{-5}{}^{+1.82\times10^{-6}}_{-1.93\times10^{-6}}$	153^{+23}_{-21}	—	$0.97^{+0.04}_{-0.04}$	$0.85^{+0.04}_{-0.04}$
$\mathrm{EFT}^{\star}_{\mathrm{A}}$ NLO II	$1.08^{+0.44}_{-0.46}$	$-1.43\times10^{-5}{}^{+2.40\times10^{-6}}_{-2.64\times10^{-6}}$	183^{+12}_{-18}	$-2.46\times10^{-3}{}^{+7.95\times10^{-3}}_{-5.48\times10^{-3}}$	$1.04^{+0.04}_{-0.04}$	$0.87^{+0.04}_{-0.04}$
$\mathrm{EFT}^{\star}_{\mathrm{B}}$ LO II	$2.76^{+0.07}_{-0.07}$	—	—	—	$1.05^{+0.05}_{-0.05}$	$0.87^{+0.04}_{-0.04}$
$\mathrm{EFT}^{\star}_{\mathrm{B}}$ NLO II	$2.63^{+0.2}_{-0.46}$	$-5.66\times10^{-7}{}^{+7.81\times10^{-7}}_{-5.01\times10^{-6}}$	397^{+74}_{-169}	—	$1.06^{+0.04}_{-0.05}$	$0.87^{+0.04}_{-0.04}$
$\mathrm{EFT}_{\mathrm{all}}$ II	$1.76^{+0.33}_{-0.51}$	$-7.42\times10^{-6}{}^{+3.02\times10^{-6}}_{-3.09\times10^{-6}}$	333^{+111}_{-134}	—	$1.02^{+0.05}_{-0.05}$	$0.91^{+0.04}_{-0.04}$
$\mathrm{EFT}_{\mathrm{A}}$ LO II	—	$-1.42\times10^{-5}{}^{+1.69\times10^{-6}}_{-1.86\times10^{-6}}$	109^{+25}_{-22}	—	$0.98^{+0.04}_{-0.05}$	$0.89^{+0.04}_{-0.04}$
$\mathrm{EFT}_{\mathrm{A}}$ NLO II	$1.23^{+0.46}_{-0.58}$	$-1.08\times10^{-5}{}^{+1.83\times10^{-6}}_{-2.27\times10^{-6}}$	160^{+23}_{-33}	$-6.59\times10^{-5}{}^{+6.53\times10^{-3}}_{-6.74\times10^{-3}}$	$1.02^{+0.04}_{-0.04}$	$0.91^{+0.04}_{-0.04}$
$\mathrm{EFT}_{\mathrm{B}}$ LO II	$2.71^{+0.07}_{-0.08}$	—	—	—	$1.02^{+0.05}_{-0.05}$	$0.91^{+0.04}_{-0.04}$
$\mathrm{EFT}_{\mathrm{B}}$ NLO II	$2.23^{+0.35}_{-0.2}$	$-3.49\times10^{-6}{}^{+2.91\times10^{-6}}_{-1.90\times10^{-6}}$	375^{+82}_{-114}	—	$1.03^{+0.04}_{-0.05}$	$0.91^{+0.04}_{-0.04}$

TABLE II. Cross sections using the prior set 1. Seed=1234

Theory	$\sigma_{23}(\mu\mathrm{b})$	$\sigma_{\mathrm{MACS}}(\mu\mathrm{b})$
$\mathrm{EFT}^{\star}_{\mathrm{all}}$ I	$4.44^{+0.32}_{-0.29}$	$6.34^{+0.39}_{-0.36}$
$\mathrm{EFT}^{\star}_{\mathrm{A}}$ LO I	$4.24^{+0.32}_{-0.28}$	$6.12^{+0.40}_{-0.37}$
$\mathrm{EFT}^{\star}_{\mathrm{A}}$ NLO I	$4.26^{+0.27}_{-0.26}$	$6.16^{+0.35}_{-0.33}$
$\mathrm{EFT}^{\star}_{\mathrm{B}}$ LO I	$3.95^{+0.18}_{-0.17}$	$5.77^{+0.26}_{-0.25}$
$\mathrm{EFT}^{\star}_{\mathrm{B}}$ NLO I	$3.92^{+0.19}_{-0.18}$	$5.73^{+0.27}_{-0.26}$
$\mathrm{EFT}_{\mathrm{all}}$ I	$3.82^{+0.45}_{-0.34}$	$5.58^{+0.58}_{-0.45}$
$\mathrm{EFT}_{\mathrm{A}}$ LO I	$3.60^{+0.38}_{-0.34}$	$5.31^{+0.52}_{-0.45}$
$\mathrm{EFT}_{\mathrm{A}}$ NLO I	$3.61^{+0.35}_{-0.29}$	$5.33^{+0.45}_{-0.41}$
$\mathrm{EFT}_{\mathrm{B}}$ LO I	$3.82^{+0.19}_{-0.19}$	$5.58^{+0.27}_{-0.28}$
$\mathrm{EFT}_{\mathrm{B}}$ NLO I	$3.63^{+0.20}_{-0.21}$	$5.33^{+0.29}_{-0.30}$
$\mathrm{EFT}^{\star}_{\mathrm{all}}$ II	$4.23^{+0.31}_{-0.29}$	$6.09^{+0.38}_{-0.38}$
$\mathrm{EFT}^{\star}_{\mathrm{A}}$ LO II	$3.87^{+0.31}_{-0.28}$	$5.64^{+0.39}_{-0.37}$
$\mathrm{EFT}^{\star}_{\mathrm{A}}$ NLO II	$3.91^{+0.28}_{-0.26}$	$5.72^{+0.37}_{-0.35}$
$\mathrm{EFT}^{\star}_{\mathrm{B}}$ LO II	$3.88^{+0.18}_{-0.18}$	$5.67^{+0.26}_{-0.27}$
$\mathrm{EFT}^{\star}_{\mathrm{B}}$ NLO II	$3.85^{+0.20}_{-0.20}$	$5.63^{+0.29}_{-0.28}$
$\mathrm{EFT}_{\mathrm{all}}$ II	$3.60^{+0.32}_{-0.25}$	$5.29^{+0.43}_{-0.35}$
$\mathrm{EFT}_{\mathrm{A}}$ LO II	$3.15^{+0.28}_{-0.25}$	$4.70^{+0.38}_{-0.35}$
$\mathrm{EFT}_{\mathrm{A}}$ NLO II	$3.37^{+0.26}_{-0.22}$	$5.00^{+0.36}_{-0.32}$
$\mathrm{EFT}_{\mathrm{B}}$ LO II	$3.75^{+0.18}_{-0.19}$	$5.48^{+0.27}_{-0.27}$
$\mathrm{EFT}_{\mathrm{B}}$ NLO II	$3.56^{+0.21}_{-0.19}$	$5.23^{+0.30}_{-0.27}$

TABLE III. Fitted parameters using the prior set 1 (Tim).

Theory	ρ (fm)	$a_1^{(2)}$ (MeV^{-3})	$r_1^{(2)}$ (MeV)	$s_1^{(2)}$ (MeV^{-1})	s_1	s_2
$\mathrm{EFT}^{\star}_{\mathrm{all}}$ I	$1.66^{+0.26}_{-0.43}$	$-1.24\times10^{-5}{}^{+2.78\times10^{-6}}_{-2.98\times10^{-6}}$	387^{+81}_{-113}	—	$1.06^{+0.05}_{-0.05}$	$0.90^{+0.04}_{-0.04}$
$\mathrm{EFT}^{\star}_{\mathrm{A}}$ LO I	—	$-2.12\times10^{-5}{}^{+1.74\times10^{-6}}_{-1.94\times10^{-6}}$	156^{+20}_{-19}	—	$1.03^{+0.05}_{-0.04}$	$0.88^{+0.04}_{-0.04}$
$\mathrm{EFT}^{\star}_{\mathrm{A}}$ NLO I	$0.56^{+0.46}_{-0.49}$	$-1.85\times10^{-5}{}^{+2.68\times10^{-6}}_{-2.95\times10^{-6}}$	177^{+16}_{-24}	$-1.69\times10^{-3}{}^{+7.14\times10^{-3}}_{-5.48\times10^{-3}}$	$1.06^{+0.04}_{-0.04}$	$0.89^{+0.04}_{-0.04}$
$\mathrm{EFT}^{\star}_{\mathrm{B}}$ LO I	$2.79^{+0.07}_{-0.08}$	—	—	—	$1.08^{+0.05}_{-0.05}$	$0.87^{+0.04}_{-0.04}$
$\mathrm{EFT}^{\star}_{\mathrm{B}}$ NLO I	$2.70^{+0.18}_{-0.46}$	$-3.71\times10^{-7}{}^{+7.54\times10^{-7}}_{-4.94\times10^{-6}}$	372^{+95}_{-167}	—	$1.08^{+0.04}_{-0.05}$	$0.88^{+0.04}_{-0.04}$
$\mathrm{EFT}_{\mathrm{all}}$ I	$1.69^{+0.40}_{-0.65}$	$-9.05\times10^{-6}{}^{+3.96\times10^{-6}}_{-4.39\times10^{-6}}$	328^{+117}_{-132}	—	$1.05^{+0.05}_{-0.05}$	$0.91^{+0.04}_{-0.04}$
$\mathrm{EFT}_{\mathrm{A}}$ LO I	—	$-1.72\times10^{-5}{}^{+2.00\times10^{-6}}_{-2.36\times10^{-6}}$	128^{+24}_{-20}	—	$1.03^{+0.05}_{-0.05}$	$0.90^{+0.04}_{-0.04}$
$\mathrm{EFT}_{\mathrm{A}}$ NLO I	$0.87^{+0.59}_{-0.70}$	$-1.37\times10^{-5}{}^{+3.06\times10^{-6}}_{-3.73\times10^{-6}}$	161^{+27}_{-35}	$-9.37\times10^{-4}{}^{+6.90\times10^{-3}}_{-5.93\times10^{-3}}$	$1.04^{+0.05}_{-0.04}$	$0.91^{+0.04}_{-0.04}$
$\mathrm{EFT}_{\mathrm{B}}$ LO I	$2.74^{+0.07}_{-0.08}$	—	—	—	$1.05^{+0.05}_{-0.05}$	$0.91^{+0.04}_{-0.04}$
$\mathrm{EFT}_{\mathrm{B}}$ NLO I	$2.31^{+0.30}_{-0.24}$	$-2.92\times10^{-6}{}^{+2.39\times10^{-6}}_{-2.18\times10^{-6}}$	344^{+105}_{-128}	—	$1.05^{+0.05}_{-0.05}$	$0.91^{+0.04}_{-0.04}$
$\mathrm{EFT}^{\star}_{\mathrm{all}}$ II	$1.75^{+0.22}_{-0.35}$	$-1.07\times10^{-5}{}^{+2.56\times10^{-6}}_{-2.81\times10^{-6}}$	398^{+71}_{-94}	—	$1.03^{+0.05}_{-0.05}$	$0.89^{+0.04}_{-0.04}$
$\mathrm{EFT}^{\star}_{\mathrm{A}}$ LO II	—	$-1.91\times10^{-5}{}^{+1.96\times10^{-6}}_{-1.90\times10^{-6}}$	154^{+23}_{-22}	—	$0.97^{+0.05}_{-0.04}$	$0.85^{+0.04}_{-0.04}$
$\mathrm{EFT}^{\star}_{\mathrm{A}}$ NLO II	$1.06^{+0.45}_{-0.44}$	$-1.45\times10^{-5}{}^{+2.44\times10^{-6}}_{-2.56\times10^{-6}}$	182^{+12}_{-18}	$-2.08\times10^{-3}{}^{+6.51\times10^{-3}}_{-5.53\times10^{-3}}$	$1.04^{+0.04}_{-0.04}$	$0.87^{+0.04}_{-0.04}$
$\mathrm{EFT}^{\star}_{\mathrm{B}}$ LO II	$2.77^{+0.07}_{-0.08}$	—	—	—	$1.05^{+0.05}_{-0.05}$	$0.87^{+0.04}_{-0.04}$
$\mathrm{EFT}^{\star}_{\mathrm{B}}$ NLO II	$2.65^{+0.17}_{-0.48}$	$-4.39\times10^{-7}{}^{+6.57\times10^{-7}}_{-4.99\times10^{-6}}$	385^{+87}_{-178}	—	$1.05^{+0.04}_{-0.04}$	$0.86^{+0.04}_{-0.03}$
$\mathrm{EFT}_{\mathrm{all}}$ II	$1.76^{+0.32}_{-0.57}$	$-7.56\times10^{-6}{}^{+2.87\times10^{-6}}_{-3.19\times10^{-6}}$	324^{+118}_{-132}	—	$1.02^{+0.05}_{-0.05}$	$0.91^{+0.04}_{-0.04}$
$\mathrm{EFT}_{\mathrm{A}}$ LO II	—	$-1.42\times10^{-5}{}^{+1.79\times10^{-6}}_{-1.76\times10^{-6}}$	107^{+22}_{-21}	—	$0.98^{+0.05}_{-0.04}$	$0.89^{+0.04}_{-0.04}$
$\mathrm{EFT}_{\mathrm{A}}$ NLO II	$1.21^{+0.49}_{-0.57}$	$-1.09\times10^{-5}{}^{+1.88\times10^{-6}}_{-2.32\times10^{-6}}$	160^{+26}_{-33}	$-1.77\times10^{-3}{}^{+7.44\times10^{-3}}_{-5.55\times10^{-3}}$	$1.01^{+0.05}_{-0.05}$	$0.90^{+0.04}_{-0.04}$
$\mathrm{EFT}_{\mathrm{B}}$ LO II	$2.71^{+0.08}_{-0.09}$	—	—	—	$1.02^{+0.05}_{-0.05}$	$0.91^{+0.04}_{-0.04}$
$\mathrm{EFT}_{\mathrm{B}}$ NLO II	$2.24^{+0.38}_{-0.21}$	$-3.53\times10^{-6}{}^{+3.06\times10^{-6}}_{-1.96\times10^{-6}}$	378^{+82}_{-110}	—	$1.03^{+0.04}_{-0.05}$	$0.91^{+0.04}_{-0.04}$

TABLE IV. Cross sections using the prior set 1 (Tim).

Theory	$\sigma_{23}(\mu\mathrm{b})$	$\sigma_{\mathrm{MACS}}(\mu\mathrm{b})$
$\mathrm{EFT}^{\star}_{\mathrm{all}}$ I	$4.44^{+0.34}_{-0.31}$	$6.35^{+0.41}_{-0.39}$
$\mathrm{EFT}^{\star}_{\mathrm{A}}$ LO I	$4.24^{+0.33}_{-0.28}$	$6.13^{+0.40}_{-0.36}$
$\mathrm{EFT}^{\star}_{\mathrm{A}}$ NLO I	$4.24^{+0.28}_{-0.26}$	$6.14^{+0.36}_{-0.34}$
$\mathrm{EFT}^{\star}_{\mathrm{B}}$ LO I	$3.96^{+0.18}_{-0.19}$	$5.78^{+0.27}_{-0.28}$
$\mathrm{EFT}^{\star}_{\mathrm{B}}$ NLO I	$3.93^{+0.21}_{-0.21}$	$5.75^{+0.30}_{-0.30}$
$\mathrm{EFT}_{\mathrm{all}}$ I	$3.83^{+0.40}_{-0.32}$	$5.59^{+0.50}_{-0.43}$
$\mathrm{EFT}_{\mathrm{A}}$ LO I	$3.60^{+0.38}_{-0.31}$	$5.32^{+0.51}_{-0.42}$
$\mathrm{EFT}_{\mathrm{A}}$ NLO I	$3.61^{+0.35}_{-0.30}$	$5.33^{+0.47}_{-0.41}$
$\mathrm{EFT}_{\mathrm{B}}$ LO I	$3.82^{+0.19}_{-0.18}$	$5.58^{+0.28}_{-0.26}$
$\mathrm{EFT}_{\mathrm{B}}$ NLO I	$3.62^{+0.20}_{-0.20}$	$5.32^{+0.28}_{-0.29}$
$\mathrm{EFT}^{\star}_{\mathrm{all}}$ II	$4.25^{+0.32}_{-0.30}$	$6.11^{+0.39}_{-0.38}$
$\mathrm{EFT}^{\star}_{\mathrm{A}}$ LO II	$3.88^{+0.31}_{-0.31}$	$5.65^{+0.39}_{-0.40}$
$\mathrm{EFT}^{\star}_{\mathrm{A}}$ NLO II	$3.93^{+0.27}_{-0.26}$	$5.75^{+0.36}_{-0.35}$
$\mathrm{EFT}^{\star}_{\mathrm{B}}$ LO II	$3.90^{+0.18}_{-0.19}$	$5.69^{+0.26}_{-0.27}$
$\mathrm{EFT}^{\star}_{\mathrm{B}}$ NLO II	$3.84^{+0.19}_{-0.18}$	$5.61^{+0.27}_{-0.26}$
$\mathrm{EFT}_{\mathrm{all}}$ II	$3.61^{+0.34}_{-0.28}$	$5.30^{+0.46}_{-0.38}$
$\mathrm{EFT}_{\mathrm{A}}$ LO II	$3.15^{+0.27}_{-0.26}$	$4.70^{+0.38}_{-0.37}$
$\mathrm{EFT}_{\mathrm{A}}$ NLO II	$3.37^{+0.25}_{-0.24}$	$5.00^{+0.36}_{-0.33}$
$\mathrm{EFT}_{\mathrm{B}}$ LO II	$3.75^{+0.19}_{-0.19}$	$5.48^{+0.28}_{-0.28}$
$\mathrm{EFT}_{\mathrm{B}}$ NLO II	$3.59^{+0.21}_{-0.19}$	$5.26^{+0.30}_{-0.28}$

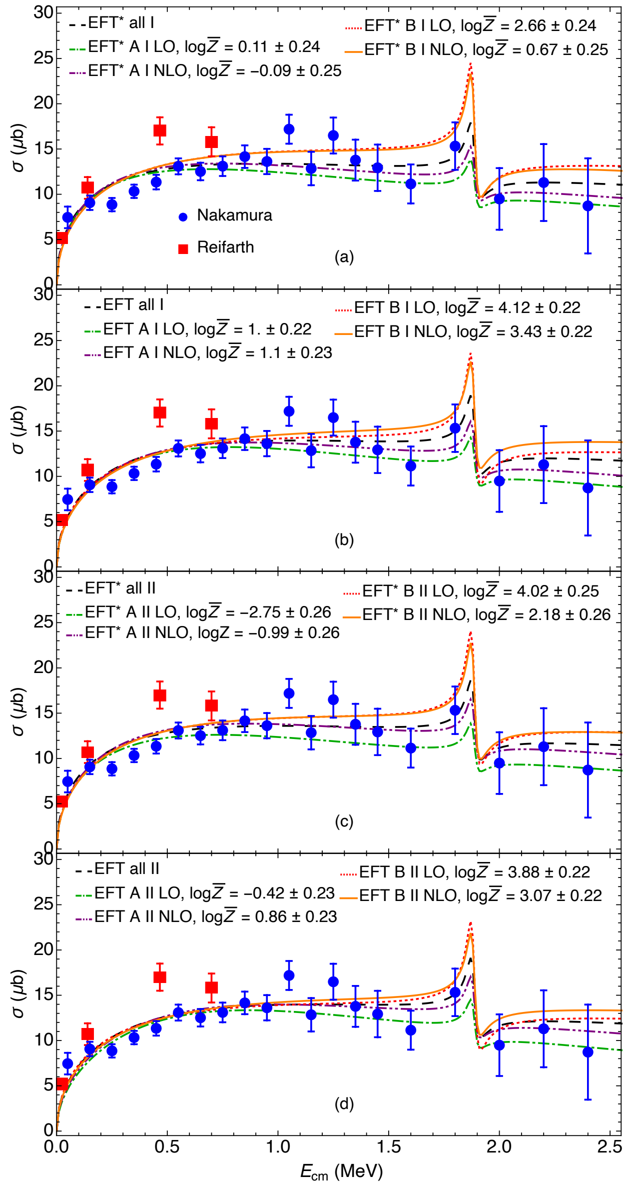

FIG. 2. ^{14}C(n, γ)^{15}C capture cross section. The dashed (black), dot-dashed (green), dot-dot-dashed (purple), dotted (red), and solid (orange) curves correspond to EFT all, EFT A LO, EFT A NLO, EFT B LO and EFT B NLO, respectively. Panel (a): Fit to all data [9, 10] around $E_{\rm cm} \leq 1\,$MeV, panel (b): Same as panel (a) except the Reifarth *et al.* data [10] at $E_{\rm cm} \leq 23.3\,$keV is not included in the fit, panel (c): fit to all data below $E_{\rm cm} \leq 2\,$MeV, and panel (d): same as panel (c) except the Reifarth *et al.* data at $E_{\rm cm} \leq 23.3\,$keV is not included. $\overline{Z}$ is the evidence for each fit normalized to the EFT all evidence.

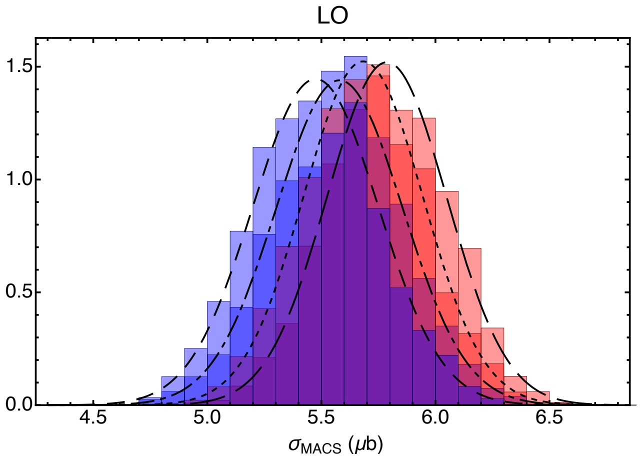

FIG. 3. $^{14}\mathrm{C}(\mathrm{n},\gamma)^{15}\mathrm{C}$ MACS cross section σ_{MACS} at $k_B T = 23.3\,\mathrm{keV}$ from LO fits.The two redish distributions correspond to EFT B fits in region I and II including the Reifarth data at $E_{\mathrm{cm}} \leq 23.3\,\mathrm{keV}$. The long-dashed and dotted curves show the Gaussian approximations to the σ_{MACS} distributions in region I and II, respectively. The two blueish distributions correspond to EFT B fits in region I and II without the Reifarth data at $E_{\mathrm{cm}} \leq 23.3\,\mathrm{keV}$. The long-short-dashed and short-dashed curves show the Gaussian approximations to the σ_{MACS} distributions in region I and II, respectively. In general including the data point at $E_{\mathrm{cm}} \leq 23.3\,\mathrm{keV}$ gives a larger average σ_{MACS}.

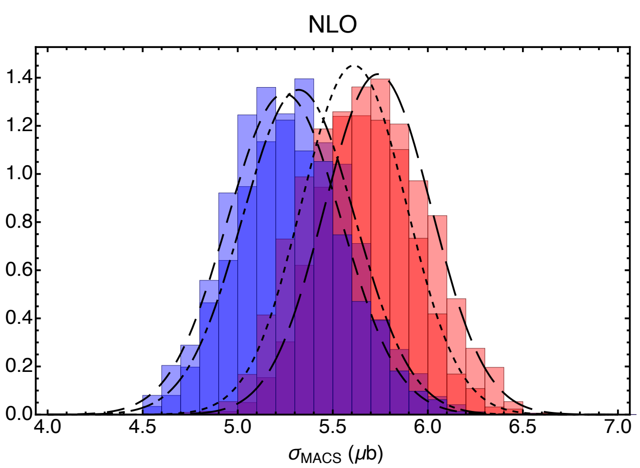

FIG. 4. $^{14}\mathrm{C}(\mathrm{n},\gamma)^{15}\mathrm{C}$ MACS cross section σ_{MACS} at $k_B T = 23.3\,\mathrm{keV}$ from NLO fit.The two redish distributions correspond to EFT B fits in region I and II including the Reifarth data at $E_{\mathrm{cm}} \leq 23.3\,\mathrm{keV}$. The long-dashed and dotted curves show the Gaussian approximations to the σ_{MACS} distributions in region I and II, respectively. The two blueish distributions correspond to EFT B fits in region I and II without the Reifarth data at $E_{\mathrm{cm}} \leq 23.3\,\mathrm{keV}$. The long-short-dashed and short-dashed curves show the Gaussian approximations to the σ_{MACS} distributions in region I and II, respectively. In general including the data point at $E_{\mathrm{cm}} \leq 23.3\,\mathrm{keV}$ gives a larger average σ_{MACS}.